# Study of Michel Spectrum of Tau Decay

by

Nicole Ackerman

Submitted to the Department of Physics
in partial fulfillment of the requirements for the degree of

Bachelor of Science in Physics

at the

MASSACHUSETTS INSTITUTE OF TECHNOLOGY

June 2007

© Nicole Ackerman, MMVII. All rights reserved.

The author hereby grants to MIT permission to reproduce and distribute publicly paper and electronic copies of this thesis document in whole or in part.

Author .....
Department of Physics
December 20, 2006

Certified by .....
Peter Fisher
Professor of Physics; Division Head, Particle and Nuclear Experimental Physics
Thesis Supervisor

Accepted by .....
David E. Pritchard
Thesis Coordinator

MASSACHUSETTS INSTITUTE OF TECHNOLOGY
AUG 0 6 2007
LIBRARIES

ARCHIVES

# Study of Michel Spectrum of Tau Decay

by

Nicole Ackerman

Submitted to the Department of Physics
on December 20, 2006, in partial fulfillment of the
requirements for the degree of
Bachelor of Science in Physics

## Abstract

This thesis is the beginning of a larger project to use BaBar to examine weak couplings through leptonic $\tau$ decay. I will use the ratio of $\mathrm{Br}(\tau \to e\nu\bar{\nu})$ and $\mathrm{Br}(\tau \to \mu\nu\bar{\nu})$ and the Michel parameters $\rho$ and $\eta$, which describe the momenta spectrum of the daughter leptons. I studied using a simultaneous fit to the $\tau \to e$ and $\tau \to \mu$ momentum spectra using $\rho, \eta$, the ratio $\mathrm{Br}(\tau \to e)/\mathrm{Br}(\tau \to \mu)$, and total number of events as the fit variables. I created a simple Monte Carlo simulation which generated a sample data spectrum and fit it for the Michel parameters $\rho$ and $\eta$. I used the Monte Carlo to assess the impact of the uncertainties in the detector response function on the measurement of the ratio $\mathrm{Br}(\tau \to e)/\mathrm{Br}(\tau \to \mu)$. My conclusion is that the three efficiency uncertainties equally have the greatest effect on the measurement of the number of events. The energy offset affects the measurement of $\mathrm{Br}(\tau \to e)/\mathrm{Br}(\tau \to \mu)$ and that the energy scale and offset uncertainties have a non-negligible effect on $\rho$ and $\eta$.

Thesis Supervisor: Peter Fisher
Title: Professor of Physics; Division Head, Particle and Nuclear Experimental Physics

# Acknowledgments

I'd like to thank my father and grandparents who always listen to me talk about physics and encourage me in everything that I do. I realize that I would not be where I am now without the encouragement and mentorship of my teachers at OSMTech and everyone on Team RUSH, especially Mrs. Hughes. I thank my sisters at $A\Phi$ for editing my papers and keeping me happy and sane.

I am very grateful toward Prof. Fisher for providing me with opportunities to do exciting research, including the topic of this thesis. I have loved working on this and learning from him. I couldn't have done this without the help of those at SLAC - especially Steve Sekula, Min Liang Zhao, and Karsten Koeneke.

This work was partially supported by the Reed Fund.

# Contents

# List of Figures

# List of Tables

# Chapter 1

# Introduction

Our understanding of the complex and fascinating world in which we live grew tremendously over the past century, due to experimental physics. New discoveries overturned contemporary models and inspired new theories. We have been led to what is called the *Standard Model*, the summation of our knowledge of particle physics. While it accurately describes the low energy phenomena that we have seen, many physicists believe that it only approximates a much more complete model of particle interactions. A complete theory would include gravity, dark-matter, inflation, and the matter-antimatter asymmetry seen in the universe. Many expect the complete theory to have more symmetries than the Standard Model, which requires 29 parameters and has patterns indicating deeper symmetries. Finally, we have yet to observe the Higg's boson, which is essential to the Standard Model. There are many theoretical models that expand on the Standard Model, such as different flavors of supersymmetry and Higgs mechanisms [3]. By making precision measurements, it is possible to observe small deviations from the Standard Model that support or exclude competing theoretical models.

## 1.1 Value of Studying the $\tau$ Branching Ratios and Michel Parameters

New experiments, such as the Large Hadron Collider, have been developed to test the standard model and look for "new physics", phenomena which can only be explained by an addition to the Standard Mode. However, results from these experiments are years away and valuable tests can currently be performed using data that is already collected and understood. The measurement of the ratio of the branching fractions of the two leptonic channels $\tau \rightarrow e\nu\bar{\nu}$ and $\tau \rightarrow \mu\nu\bar{\nu}$ and the energy distribution of the daughter leptons are examples of the windows into the Standard Model provided by leptonic $\tau$ decay. These results would improve our understanding of the weak interaction and could reveal hints of new physics.

Lepton universality predicts the branching fractions of $\tau \rightarrow \mu\nu\bar{\nu}$ and $\tau \rightarrow e\nu\bar{\nu}$ are equal with some small, calculable quantum corrections due to mass differences between the electron and muon. By measuring the ratio more accurately, constraints are put on these corrections. One use of this is to test the NuTeV measurements of the weak mixing angle, which disagreed with the Standard Model values by 3 $\sigma$. One of the NuTeV proposals is a family dependent suppression of the $W\ell\nu_\ell$ coupling by a factor of (1-$\epsilon_\ell$/2) where $\epsilon_\ell$ parameterizes violation of universality coming from the interaction of heavier particles [4, 5]. This NuTeV measurement and its implications will be discussed further in section 2.1.1.

The energy distribution of the daughter leptons from $\tau$ decay can be described by the Michel parameters. The Michel parameters ($\rho$ and $\eta$) are functions of the charged current coupling constants ($g^{\kappa}_{\epsilon\lambda}$, $\kappa \in \{S, V, T\}$ and $\epsilon, \lambda \in \{R, L\}$ ) of the weak interaction and will be explained in section 2.2. Non-Standard Model values for the Michel parameters would imply a more complex structure to the weak interaction than currently believed, or other new physics. The parameter $\eta$ is related to the partial decay width of the $\tau$ assuming lepton universality, and additional charged Higgs bosons would be needed to explain any deviation of $\eta$ from the Standard Model value [6].

## 1.2 Using BaBar to Study $\tau$ Physics

Studies of the branching ratios and the Michel parameters have been done on other experiments in recent years ([7, 8]), but BaBar has the potential to yield much better statistics than the previous studies. BaBar is the detector at the SLAC $B$-Factory, where the primary interaction of interest is $e^+e^- \rightarrow \Upsilon(4S) \rightarrow B\bar{B}$, with a cross-section of 1.05 nb. But $e^+e^- \rightarrow \Upsilon(4S) \rightarrow \tau^-\tau^+$ has a relatively high cross-section of 0.89 nb, making the BaBar experiment a $\tau$ factory as well [9].

A preliminary study was done with the first year of BaBar data in 2001 to measure the branching ratio of the leptonic channels. Using 0.828 fb$^{-1}$ of data, which corresponds to about $7.3\times10^5$ $\tau$ pairs, the value of the ratio of the gauge couplings was determined to be

$$\frac{g_\mu}{g_e} = 0.979 \pm 0.021 \tag{1.1}$$

which is consistent with the standard model prediction of 1.0. While the uncertainty was quite large in comparison to the world average of $1.0010 \pm 0.0020$, this was only a preliminary study [10].

The study concluded that a competitive measurement of the branching ratio could be achieved with the full data set, but there were many sources of uncertainty highlighted. One concern was the multiplicity of hadronic events that would pass the 3-1 topology cut, requiring one hemisphere to have 3 tracks and the other to have 1 track, where a hemisphere is defined by the thrust of the event. The analysis was instead performed with a 1-1 topology, looking for one track in each hemisphere. A source of systematic error is the difference in tracking efficiencies in the drift chamber for muons and electrons. There was also a contribution from the uncertainty in the luminosity and the reduced efficiency of the muon system, which has since been replaced. In order to deal with backgrounds (such as $\pi$), a number of specific cuts and filters were made for the analysis. The spectrum was broken into three regions to calculate the ratio, in order to account for the fact that the $\pi$ contamination is a function of momentum.

### 1.2.1 New Approach: Michel Spectrum

This analysis can be improved by reducing backgrounds and systematic errors by using the Michel parameters as constraints. The branching ratio is equal to the ratio of the integrals of the muon and electron energy spectra from tau decays. Uncertainties in detector efficiency and luminosity cancel if they effect both leptons equally. A simultaneous fit can be done to four fit parameters: the Michel parameters $\rho$ and $\eta$, the number of electron events, and the ratio of the number of muon to electron events.

The Michel parameters are constrained to be equal in the two leptonic spectra. This will constrain the shape of the entire spectra, reducing the influence of backgrounds and misidentification that haven't been corrected for and only occupy a certain momentum region. This constraint will provide additional information during the development of the analysis since large uncertainties in the fit parameters could indicate poorly modeled data.

The values of the Michel parameters are important in their own right, in addition to improving the measurement of the branching ratio. The current world averages of are consistent with the Standard Model. The parameters are related to the gauge couplings and a measurement inconsistent with the Standard Model would indicate new physics contributions to the weak interaction.

The measurement will be done with over $3 \times 10^8$ $\tau$ pairs, corresponding to the integrated luminosity of 375 fb$^{-1}$ from Runs 1-5. The $\tau$ events will be selected based on thrust, energy, charge, and particle identification. We will use a 3-1 topology, requiring a charged lepton in the single prong hemisphere, but not in the other hemisphere. This corresponds to requiring one $\tau$ to decay leptonically and the other to decay hadronically. The branching fraction of $\tau^- \to h^-h^-h^+$ is 15.19±0.07 [2], so this is will not significantly reduce our signal, but will drastically reduce the contamination from Bhabha and dimuon events being misidentified as $\tau^+\tau^-$ events. Only drift chamber data will be used to measure momentum in order to cancel uncertainties between the electron and muon decays. The Monte Carlo that will be used for fitting

is produced with the Standard Model values for $\rho$ and $\eta$. Events will be assigned a weight that can be modified to account for non-Standard Model values of the Michel parameters.

While there will be systematic errors introduced due to selectors and other analysis methods, one important contribution to the systematic errors will be the detector response's affect on the Michel spectrum. The Monte Carlo data used for fitting will be dependent upon the model of the detector parameters, such as resolution and efficiency. which are all known within a given error from other processes. The differences between the actual parameters and how they are modeled will change the shape of the Michel spectrum. We need to establish the effect that these errors will have, and check that they can be known to a margin to make this method of analysis feasible.

# Chapter 2

# Physics

In this chapter I will discuss the relevant physics to this study. The elegance of this project is in apparently simple results leading to much subtler conclusions. The weak interaction and possible new physics can be probed through a ratio of the number of $\tau \rightarrow e$ and $\tau \rightarrow \mu$ decays. The energy spectra can be parameterized by only two numbers, yet these two numbers probe deeply into the structure of the weak interaction.

## 2.1 The Weak Interaction and Tau Lepton

The $\tau$ is the heaviest of the known charged leptons and is identical to them in every way except mass. Table 2.1 summarizes some of the important properties of the $\tau$ lepton. While it wasn't detected until 1976 [11], it had been theoretically described in 1971 [12]. The $\tau$ is invaluable to study since it behaves identically to the well-understood electron and muon, yet allows access to interesting physics as it is the only lepton that has a large enough mass to decay hadronically. Less than half of the decays of the $\tau$ are fully leptonic, but these are understood very well due to their similarity to the decay of the muon. The $\tau$ is optimal for studying both hadronic and leptonic weak couplings because it provides a clean and well understood vertex in the production of the $W^{\pm}$ [13].

Quarks and leptons decay through the weak interaction; the first evidence of it was

Table 2.1: Properties of the $\tau$ lepton [2].

| | |
|---|---|
| Mass | $m = 1776.99^{+0.29}_{-0.26}$ MeV |
| Mean Life | $\tau = (290.6 \pm 1.1) \times 10^{-15} s$ |
| Branching Fraction $\mu^- \bar{\nu}_\mu \nu_\tau$ | $(\Gamma_\mu/\Gamma) = (17.36 \pm 0.06)\%$ |
| Branching Fraction $e^- \bar{\nu}_e \nu_\tau$ | $(\Gamma_e/\Gamma) = (17.84 \pm 0.06)\%$ |

through nuclear $\beta$-decay. Weak interactions proceed through the *charged* and *neutral currents*, mediated by the $W^\pm$ and $Z^0$ bosons, respectively. The weak interaction allows flavor change in leptons and quarks. A $W^\pm$ boson exchange results in a lepton transforming into the neutrino of its family $(e, \mu, \tau)$ and the production of a charged lepton and its antineutrino (or antilepton and neutrino). The change in charge is one unit, corresponding to the charged current. The $W^\pm$ and $Z^\circ$ bosons also can mediate semileptonic and non-leptonic processes, however, the decays I am studying are fully leptonic. [14]

The Glashow-Weinberg-Salam model unified the electromagnetic and weak interactions through mixing of a Boson from the weak isospin triplet ($W^0$) with one from the isospin singlet ($B^0$),

$$\begin{aligned} |\gamma\rangle &= \cos\theta_W |B^0\rangle + \sin\theta_W |W^0\rangle \\ |Z^0\rangle &= -\sin\theta_W |B^0\rangle + \cos\theta_W |W^0\rangle \end{aligned} \tag{2.1}$$

to produce the massless photon and massive $Z^0$ boson. $\theta_W$ is the weak mixing angle, or Weinberg angle. One way to measure $\theta_W$ is through the mass ratio of the $W^\pm$ and $Z^\pm$ bosons which is given by $\cos\theta_W$. Another method is through measurement of the coupling constants, as my study has the potential to do. [14, 13]

Two of the notable properties of the weak interaction is its limited range ($\hbar c/M_W \sim 10^{-3}$fm) and parity violation. Parity is related to the property of helicity, defined as

$$h = \frac{\vec{s} \cdot \vec{p}}{|\vec{s}| \cdot |\vec{p}|} \tag{2.2}$$

where $\vec{s}$ is the spin of the particle and $\vec{p}$ is the momentum. Spin is an axial quantity and momentum is a vector quantity. Particles can either be left- or right-handed, with helicity changing signs under the parity operator. An operator that conserves parity will couple identically to both handednesses. Any exchange of a spin-1 particle can be described by an operator with axial and vector components. For it to conserve parity, it must either be purely axial or purely vector. In parity violating interactions, both parts are present and described by the coefficients $c_V$ and $c_A$. Maximum parity violation occurs when $c_V = \pm c_A$, correspondingly called V-A and V+A interactions. Experimental results yield $c_V = -c_A = 1$, which implies the weak interaction is V-A and only couples to left-handed fermions and right-handed antifermions. The V+A interaction is responsible for coupling to right-handed fermions and left-handed antifermions, which has yet to be seen in charged current interactions [13].

The general, Lorentz invariant, four-lepton interaction matrix element for leptonic decay of the $\tau$ is given by

$$\mathcal{M} = 4\frac{G_F}{\sqrt{2}} \sum_{\substack{\kappa=S,V,T \\ \epsilon,\lambda=R,L}} g^{\kappa}_{\epsilon\lambda} \left\langle \bar{\psi}_{\epsilon}(\ell)|\Gamma^{\kappa}|\psi_{\rho}(\nu_{\ell})\right\rangle \left\langle \bar{\psi}_{\omega}(\nu_{\tau})|\Gamma^{\kappa}|\psi_{\lambda}(\tau)\right\rangle \tag{2.3}$$

where $\kappa$ labels the types of interactions (scalar, vector, or tensor) and $\epsilon$ and $\lambda$ label the handedness of the charged leptons [6]. There are 10 possible coupling constants ($g^{\kappa}_{\epsilon\lambda}$), for which the Standard model predicts all are zero, except for $g^{V}_{LL} = 1$. This corresponds to assuming a V-A structure for the weak interaction. If it could be shown that any of the other coupling constants were non-zero, it would indicate new physics; a more complex structure of the weak interaction, either through changes in the couplings to the W-boson or through new gauge bosons [7].

### 2.1.1 The NuTeV Anomaly

The NuTeV experiment at Fermilab measured the ratio of neutral current to charged current event in muon neutrino-nucleon and antineutrino-nucleon scattering. $g^2_L$ were found to be $3\sigma$ smaller than the Standard Model prediction from the neutrino-quark

coupling constants. One proposed explanation for this discrepancy is a suppression (by factor $\epsilon$) of the $Z^0$ and $W^{\pm}$ bosons to the neutrino and a heavy Higgs boson [4]. Additionally, the lepton universality ($g_\ell/g'_\ell$) must be modified by $\epsilon$ as well. Assuming independence of the three $\epsilon_\ell$, the NuTeV results, combined with all other electroweak results give

$$\begin{aligned} \epsilon_e &= 0.0048 \pm 0.0018 \\ \epsilon_\mu &= 0.0027 \pm 0.0014 \\ \epsilon_\tau &= 0.0007 \pm 0.0028 \end{aligned}$$

The ratios of the coupling constants are given by $\frac{g_\ell}{g'_\ell} \approx 1 + \frac{\epsilon'_\ell - \epsilon_\ell}{2}$, which all can be determined from the leptonic decays of the $\tau$ [5].

From the NuTeV results, a measurement of the weak mixing angle (Eq. 2.1) was made that was a factor of two more precise than previous measurements. However, this value was $3\sigma$ from the expected Standard Model value. There are multiple possibilities to explain this discrepancy, including a heavy Higgs, strange sea asymmetry, or extra Z' bosons. All of these are relatively exotic modifications to the Standard Model, making any verification of the NuTeV measurement of $\theta_W$ very interesting [15].

## 2.2 Michel Spectrum

In 1949 Louis Michel postulated a parameterization of the energy spectrum of the electrons produced in "$\mu$-meson" (now known as the $\mu$ lepton) decays based upon the interaction matrix [16]. This spectrum is still accurate, though the understanding of the underlying physics has vastly improved. The energy distribution is dependent upon the matrix elements of the interactions matrix given in Eq. 2.3. There are four "Michel Parameters" that can be created from these coupling constant, simplifying

the expression to:

$$\frac{d^2\Gamma_{\tau\to\ell\nu_\ell\nu_\tau}}{d\Omega dx} = \frac{G_0^2 m_\tau^5}{192\pi^4}x^2\Bigg\{3(1-x)+\rho_\ell\left(\frac{8}{3}x-2\right)+6\eta_\ell\frac{m_\ell}{m_\tau}\frac{(1-x)}{x} \\ -P_\tau\xi_l\cos\theta\left[(1-x)+\delta_\ell\left(\frac{8}{3}x-2\right)\right]\Bigg\} \tag{2.4}$$

where $x = E_\ell/E_\ell^{max}$ in the $\tau$ rest frame and $\cos\theta$ is the angle between $\tau$-spin and the momentum of the daughter lepton. The Michel parameters are related to the charged current couplings by

$$\rho = \frac{3}{4}|g_{LL}^V|^2+\frac{3}{4}|g_{RR}^V|^2+\frac{3}{16}|g_{LL}^S|^2+\frac{3}{16}|g_{LR}^S|^2+\frac{3}{16}|g_{RL}^S|^2+\frac{3}{16}|g_{RR}^S|^2+ \\ \frac{3}{4}|g_{LR}^T|^2+\frac{3}{4}|g_{RL}^T|^2-\frac{3}{4}Re\left(g_{LR}^S g_{LR}^{T*}\right)-\frac{3}{4}Re\left(g_{RL}^S g_{RL}^{T*}\right), \tag{2.5}$$

$$\eta = \frac{1}{2}Re\left(6g_{LR}^V g_{LR}^{T*}+6g_{RL}^V g_{RL}^{T*}+g_{RR}^S g_{LL}^{V*}+g_{RL}^S g_{LR}^{V*}+g_{LR}^S g_{RL}^{V*}+g_{LL}^S g_{RR}^{V*}\right), \tag{2.6}$$

$$\xi = |g_{LL}^V|^2+3|g_{LR}^V|^2-3|g_{RL}^V|^2-|g_{RR}^V|^2+5|g_{LR}^T|^2-5|g_{RL}^T|^2+ \\ \frac{1}{4}|g_{LL}^S|^2-\frac{1}{4}|g_{LR}^S|^2+\frac{1}{4}|g_{RL}^S|^2-\frac{1}{4}|g_{RR}^S|^2+4Re\left(g_{LR}^S g_{LR}^{T*}\right)-4Re\left(g_{RL}^S g_{RL}^{T*}\right), \tag{2.7}$$

$$\xi\delta = \frac{3}{4}|g_{LL}^V|^2-\frac{3}{4}|G_{RR}^V|^2+\frac{3}{16}|g_{LL}^S|^2-\frac{3}{16}|g_{LR}^S|^2+\frac{3}{16}|g_{RL}^S|^2-\frac{3}{16}|g_{RR}^S|^2+ \\ -\frac{3}{4}|g_{LR}^T|^2+\frac{3}{4}|g_{RL}^T|^2+\frac{3}{4}Re\left(g_{LR}^S g_{LR}^{T*}\right)-\frac{3}{4}Re\left(g_{RL}^S g_{RL}^{T*}\right). \tag{2.8}$$

Plugging in $g_{LL}^V = 1$ and all other constants set to zero, the Standard Model predicts the values are $\rho = 3/4$, $\eta = 0$, $\xi = 1$, and $\delta = 3/4$ ($\xi\delta = 3/4$)[7].

The parameters $\xi$ and $\delta$ are accessible either by polarizing the $\tau$ or measuring the polarization of the final state lepton, which was not of part of this study. From Eq. 2.4 it can be seen that the polarized term is independent and can be ignored by integrating over all $\theta$. Hence, the spectrum is only dependent upon the two parameters $\rho$ and $\eta$. It is worthwhile to note that some measurements of new physics are dependent upon the polarized measurements as well [17] and that it is possible

to make these measurements using BaBar using the correlation between $\tau$ decays.

Assuming universality between $\mu$ and $e$ and $\eta_\mu = \eta_e$, $\eta$ can be expressed as

$$\eta = \frac{1}{4}\frac{m_\tau}{m_\mu - m_e}\left[\frac{B(\tau^- \to \mu^-\bar{\nu}_\mu\nu_\tau)}{B(\tau^- \to e^-\bar{\nu}_e\nu_\tau)} - (1 + (\Delta_\mu - \Delta_e))\right] \tag{2.9}$$

where $\Delta_\ell$ are small corrections, $\Delta_\mu = -0.031$ and $\Delta_e = -0.004$, due to the lepton masses, QED radiative corrections, and the boson propagator [6]. The Standard Model prediction is $\eta$=0, which is a result of universality predicting the branching fraction to be equal (except for the corrections). If measurements of $\eta$ and the branching ratio of the leptonic decays do not agree, then either the universality assumption is incorrect or there are other corrections possibly due to new physics.

If the charged weak interaction has other contributions to leptonic decay structure, the decay of the $\tau$ will be the best place to look, due to mass-dependent couplings. The leptonic decay channels are ideal since the electroweak couplings can be studied without disturbances from the strong interaction [7].

One of the terms in the expression for $\eta$ is the interference term of $\tau_R^- \to \ell_R^-\nu_{\tau L}\bar{\nu}_{\ell R}$, which occurs through a charged Higgs boson and appears in certain extensions of the standard model. If the charged Higgs is the only modification to $\tau$ decay [6],

$$\eta = -\frac{m_\tau m_\mu \tan^2\beta}{2m_H^2} \tag{2.10}$$

For $\tan\beta = 5$ and $M_H = 100\text{GeV}$, $\eta \approx 2.32 \times 10^{-4}$.

Additionally, as mentioned in section 2.1.1, the original NuTeV results indicate new physics, such as lepton non-universality. The relationship between the Michel parameters and the branching ratio can help determine whether the new physics lies in non-universality.

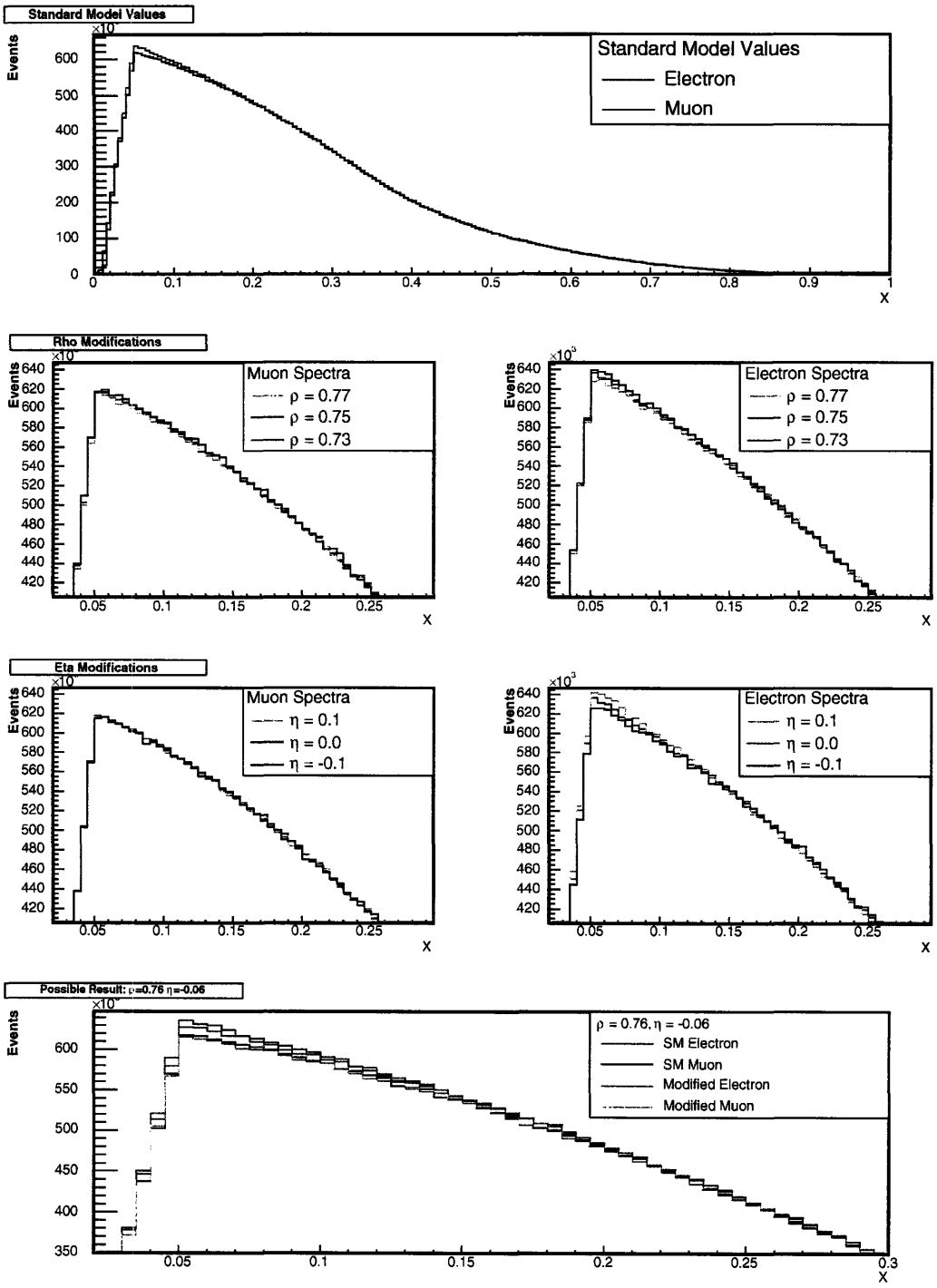


Figure 2-1: The top plot is of Standard Model values of $\rho$ and $\eta$, the four underneath show the effect of changing $\rho$ and $\eta$ individually, and the bottom plot shows the difference between Standard Model and one possible alternative spectrum.

# Chapter 3

# BaBar Experiment

## 3.1 The PEP-II Accelerator

The PEP-II asymmetric B Factory has been operating since May of 1999. The accelerator produces a 9.0 GeV electron beam and a 3.1 GeV positron beam with a center of mass energy of 10.58 GeV. This corresponds to the $\Upsilon(4S)$ resonance that has a branching fraction to $B\bar{B}$ of 0.96 [2]. The asymmetric beams provide a Lorentz boost of $\gamma = 0.56$ in order to adequately separate the B mesons produced for CP violation studies. PEP-II has operated at a peak luminosity of 10.88 $\times 10^{33}\text{cm}^{-2}\text{s}^{-1}$, which far surpasses the design luminosity of $3.00\times 10^{33}\text{cm}^{-2}\text{s}^{-1}$. It has delivered a total integrated luminosity (as of June 2006) of over 375 $\text{fb}^{-1}$ [18].

## 3.2 The BaBar Detector

The BaBar detector was designed to exploit the potential of PEP-II, specifically to measure the CP violations in the decay of B mesons to their CP eigenstates. This placed many requirements on the design [1]. The final detector design consists of an inner detector surrounded by a 1.5T solenoid and instrumented flux return. The inner detector is comprised of a silicon vertex track, drift chamber, ring-imaging Cerenkov detector, and calorimeter.

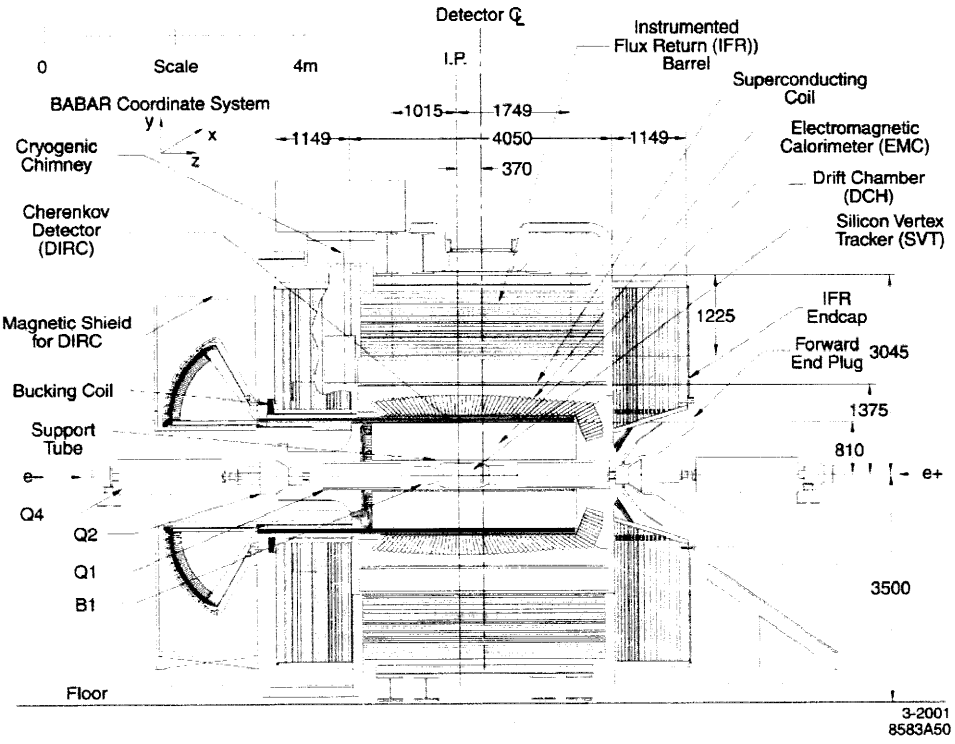


Figure 3-1: The BaBar detector (from [1])

### 3.2.1 Drift Chamber System

The drift chamber system (DCH) measures the momentum for charged particles, provides a trigger for charged particles, and measures dE/dx. An energetic charged particle ionizes the gas in the chamber as it passes through. The electrons drift in a electric field and are collected by a signal wire. The distance of closest approach is determined by the time delay in the ionization electrons reaching the signal wire. The signals from many wires are used to reconstruct the path of the particle as it travels away from the interaction point.

The central drift chamber is a cylinder with inner radius of 23.6 cm, outer radius of 81 cm, and length of 280 cm. The chamber is filled with a helium-isobutane 80:20 gas mixture. The chamber is comprised of 7104 hexagonal cells, arranged in 10 super-layers. Each super-layer contains 4 cells, arranged in an axial or stereo orientations. The typical dimension of a cell is 1.2 $\times$ 1.8 cm$^2$. Each cell is a 20 $\mu$m gold-plated tungsten-rhenium signal wire at 1960 V surrounded by 6 gold-plated aluminum wires.

The design requirements included use of light materials and precision measurements of track location and dE/dx. The inner cylinder corresponds to 0.28% $X_0$, the outer cylinder corresponds to 1.5% $X_0$, and the gas and wires account for 0.3% $X_0$ (for 90°). From prototype measurements, the BaBar drift chamber system is predicted to have a dE/dx resolution of 6.8% for 40 measurements [19]. The drift velocity in the center of the cell is 25 $\mu$m/nsec and the threshold is $< 3e^-$ [20]. The average spatial resolution across the entire cell is 125 $\mu$m. The resolution of the transverse momentum is $\sigma(p_T)/p_T \approx 0.45\% + 0.13\% \times p_T$ [21]. The dE/dx in the DCH is calculated from the total charge deposited on the wires and is used to identify particles in the momentum range of 400-1000 MeV[1].

### 3.2.2 Other Detector Subsystems

The silicon vertex tracker (SVT) is made of 5 layers of silicon strip detectors. The three innermost layers provide high precision vertex information in the form of angle and position, the outer two layers serve to link SVT and DCH measurements. It detects short-lived particles by locating the vertex of the decay tracks outside of the interaction point with a resolution of about 60 $\mu$m. The detector of internally reflected Cherenkov light (DIRC) provides differentiation between pions and kaons between 500 MeV and 4.5 GeV, as well as general energy measurements for particles above the threshold energy. The Cherenkov light is produced in silica bars 4.9 m long with a refractive index of 1.474 and is internally reflected to be detected in an array of photomultiplier tubes. The velocity of the particle is measured through the opening angle of the light cone, with an angular resolution of 2.5 mrad. The electromagnetic calorimeter (EMC) detects and measures the electromagnetic showers in the region of 20 MeV to 4 GeV. It is made of CsI(Tl) crystals read out by silicon PIN diodes. It provides electron and hadron separation and measures photon energy down to about 20 MeV. Its angular resolution in $\phi$ and $\theta$ is 3.9 mrad and its energy resolution is $\sigma_E/E = 3.0\%$. The instrumented flux return (IFR) identifies muons and neutral hadrons with resistive plate chambers in between layers of steel absorbers [1].

## 3.3 Tau Events

BaBar is well suited for $\tau$ analysis. The excellent resolution and particle identification that has allowed BaBar to study B-meson events will allow for precision $\tau$ measurements as well. The 375 $fb^{-1}$ of data collected through Run 5 corresponds to about $3.3 \times 10^8$ $\tau$ pairs. In this sample we should have about 57 (59) million events that includes at least one $\tau \rightarrow e(\mu)$ decay. I will be selecting events based on a 3-1 topology that requires the 3-prong hemisphere to not include the lepton I am looking for in the 1-prong hemisphere. This constraint will reduce the sample to about 8.9 (8.7) million electron (muon) decays. Previous measurements of the branching ratio have been made with far fewer events: the L3 collaboration used 163.256 $\tau$ events for their study in 2001 [22].

The BaBar sample is large enough that the uncertainty on any measurement will be dominated by systematic errors. A measurement of the $\tau$ lifetimes was done with 80.0 $fb^{-1}$ of BaBar data using similar topology. Only 0.44% of their initial sample of $\tau^+\tau^-$ events passed all of their cuts, which were optimized for sample purity. After correcting for differences in particle identification requirements, this would correspond to 502,000 (485,000) electron (muon) events in the analysis sample. This yields a statistical uncertainty of about $\sigma_{stat} = 0.14\%$. This is about half of the uncertainty on the current world average and is smaller than any single experiment's statistical average [2]. The additional fit constraint of the Michel spectrum would reduce the need for an extremely pure sample, allowing for a greater efficiency in selecting events, a larger sample size, and smaller statistical uncertainty. It is more important to reduce the systematic errors to be on the same scale as the statistical errors than to further reduce the statistical errors. The total error can best be minimized through a thorough understanding of the sources of the systematic errors, such as the detector response.

# Chapter 4

# Feasibility Study and Systematic Errors

I created a simple Monte Carlo program in order to study the effect of deviations between actual and modeled detector performance on the Michel parameter fit. This program modeled the detector response with 6 variables and then performed a fit between two momentum spectra resulting from leptonic $\tau$ decay. The detector response is mismatched between the "data" and "fit" spectra to examine the resulting change in the fit parameters. The data spectrum is generated from specified Michel parameters; the fit is done by varying the weights of the events in the fit spectrum based upon changing the Michel parameters. This chapter will explain the methodology used in the statistical study I performed.

## 4.1 Monte Carlo to generate Events

Each event being modeled has the form of $\tau \rightarrow \mu\nu_\tau\bar{\nu}_\mu$ where the $\tau$ is produced by $e^+e^- \rightarrow \tau^+\tau^-$. While the final quantities of interest are the properties of the $\mu$ *as measured by the detector*, the event simulation needs to begin with the $\tau$.

The $\tau$ is generated in the center of mass frame from $e^+e^- \rightarrow \tau^+\tau^-$. Neglecting radiative effects, each $\tau^\pm$ must have half of the center of mass energy and be equal and opposite in momentum. If the final state includes a hard photon, either the

energy of the $\tau$ could be modified to account for the radiation or else the event could be discarded. The coordinate system is oriented with $\phi$ defined as zero horizontally (away from the center of the PEP-II ring) increasing upward and $\theta$ defined as zero in the direction of the high energy $e^-$ beam [23]. The angle $\phi$ is sampled isotropically from a [0,2$\pi$] distribution. The angle the $\tau$ is produced at with respect to the beam axis ($\theta$) is selected from a $1 + \cos^2\theta$ distribution. The magnitude of momentum is determined from the energy ($E_{beam}/2$) and the mass of the $\tau$, $m_\tau$ = 1.77 GeV. Boosting into the $\tau$ rest frame, the muon is similarly created. $\phi$ is again isotropic in [0,2$\pi$] and $\cos\theta$ is isotropic in [-1,1].

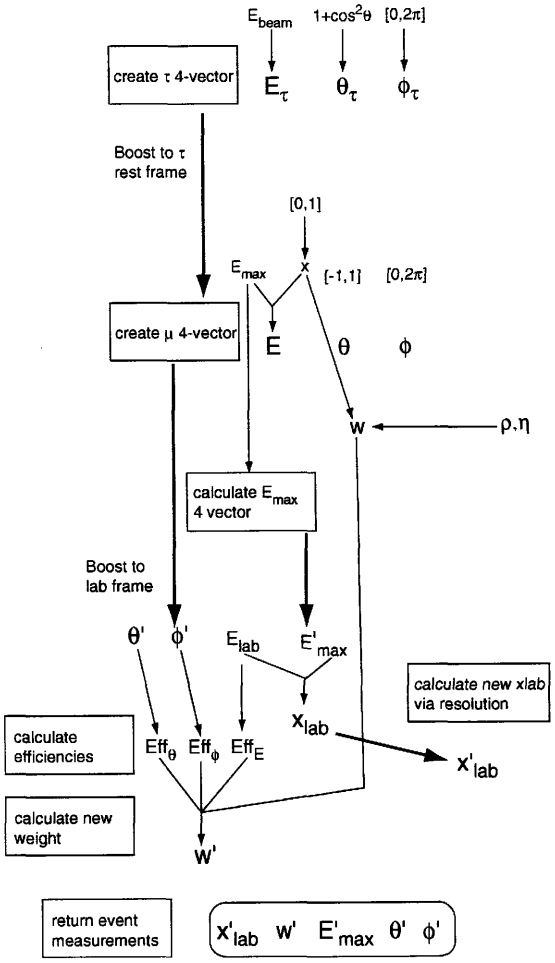


Figure 4-1: Flow of the generation of a single $\tau$ event.

The first interesting step is the generation of the energy of the muon, which is determined by the Michel spectrum. The energy is sampled from a flat distribution from zero to the maximum energy. The maximum energy that the daughter muon can have is given by

$$E_{max} = \frac{m_\mu^2 + m_\tau^2}{2m_\tau} \qquad (4.1)$$

The variable $x$ will be used to represent $x = E/E_{max}$, having possible values between 0 and 1. I will use a *Michel weight* to modify this flat energy spectrum to the physically accurate Michel spectrum. The Michel weight is dependent upon the Michel parameters, which will be modified during the fitting process. Changing the parameters will change all of the weights, which will then change the final spectrum.

The muon 4-vector is boosted from the

| Parameter | Domain | Parameterization |
|---|---|---|
| Energy | E < 45 MeV | 0 |
| | 45 MeV < E < 450 MeV | $(\epsilon_{max} \times (E - 45))/(450 - 45)$ |
| | E > 450 MeV | $\epsilon_{max}$ |
| $\phi$ | all $\phi$ | $\epsilon_{max}$ |
| $\theta$ | $\theta < \frac{\pi}{4}$ | $\epsilon_{max} \times \frac{\theta}{\pi/4}$ |
| | $\theta > \frac{\pi}{4}$ | $\epsilon_{max}$ |

Table 4.1: Modeling of the three efficiencies based on the measured parameters

$\tau$ rest frame to the center of mass frame using the $\gamma$ and angle from the $\tau$ 4-vector. It is then boosted to the lab frame by using the $\gamma$ of the beam. In the lab frame we now have the energy and momentum. We are also interested in the $x$ value in this frame. $E_{max}$ in the lab frame is calculated by creating a 4-vector in the $\tau$ rest frame that has the momentum of the muon oriented along the beam axis. Boosting this into the lab frame provides the $E_{max}$. $x_{lab}$ is simply $E/E_{max}$ and will be within [0,1].

While the true properties of the muon have been generated, the detector response now needs to be taken into account. The detector has a non-unity probability in detecting the event with respect to the energy, $\theta$, and $\phi$. The efficiencies are modeled as shown in table 4.1.

A new weight for the event is calculated by multiplying the Michel weight by the three efficiencies. Then the measured energy is calculated via $E' = aE+b$ where $a$ is a scaling value and $b$ is an offset, presumably close to one and zero, respectively. Finally, the measured energy is affected by the resolution of the detector. The measured energy is selected from a Gaussian distribution centered at the true energy and with a width of $\sigma(E)$. The values that are known for the event are then $\theta$, $\phi$, $E'$, and the weight.

The only difference in generating the data or fit spectra is in the Michel weight. The Michel parameters are fixed for the data spectrum so the Michel weight is constant. I specify what values of efficiency, energy offset, scaling, and resolution are used in each spectrum. After the generation process, the data spectrum is treated as if it is "real" data and only the *measured* $\theta$, $\phi$, $E'$, and weight is used in fitting. I

can see what the result would be if the value of (for example) the energy offset for the detector in the full BaBar Monte Carlo program was wrong by a given amount by specifying slightly different values in the two spectra for the energy offset.

## 4.2 Fitting

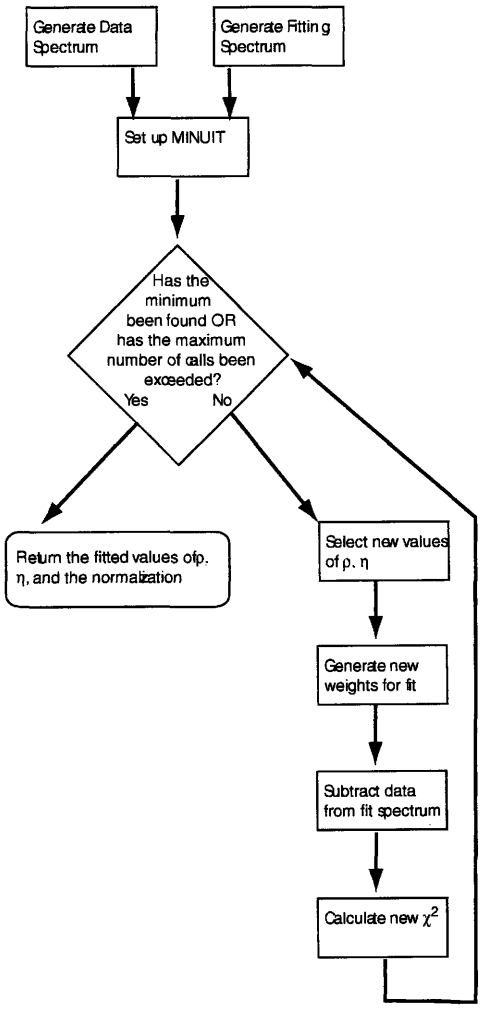


Figure 4-2: Diagram of how the data is fit for the values of $\rho$, $\eta$, and the normalization.

Fitting is done using the MINUIT package [24], which has been integrated into ROOT [25]. The fit process is outlined in Fig. 4-2. The initial set-up requires specifying beginning parameters, step sizes, the tolerance for finding the minimum, and the function of which to find the minimum. For this function, I used the reduced $\chi^2$ of the fitting spectrum to the data spectrum. MINUIT would pass new parameters to the function, which would return the $\chi^2$. The machinery of MINUIT would determine which parameter values to pass and at what point the minimum was found.

In the spectra that I was comparing, my three fitting parameters were $\rho$, $\eta$, and a normalization between the two spectra. The normalization is simple, applying a vertical scaling to the spectra. However, fitting the Michel parameters is more difficult since the probability of each event is dependent on what the parameters are. However, the shape of the curve can be changed by recalculating the weight of each event according to the new Michel parameters.

In order to minimize the time necessary for fitting, the goal is to not need to recal-

culate all weights for every fitting iteration. Instead, multiple weights are recorded for each event in the initial generation of the fitting spectrum and the fit just interpolated between these weights. This is simply a two dimensional Taylor expansion around the standard model values. The accuracy of this method is dependent upon whether the final fit value falls inside of the points used for the expansion, the amount of change in the values over the distance between sample points, and the number of terms used. My final fit included up to the third derivative, which was only slightly different from the results gained from the second derivative, implying higher order terms would be negligible. The 10 weights recorded corresponded to the weights at the expansion point (Standard Model values) and appropriate combinations of $\rho$ and/or $\eta$ shifted by 1, 2, or 3 increments.

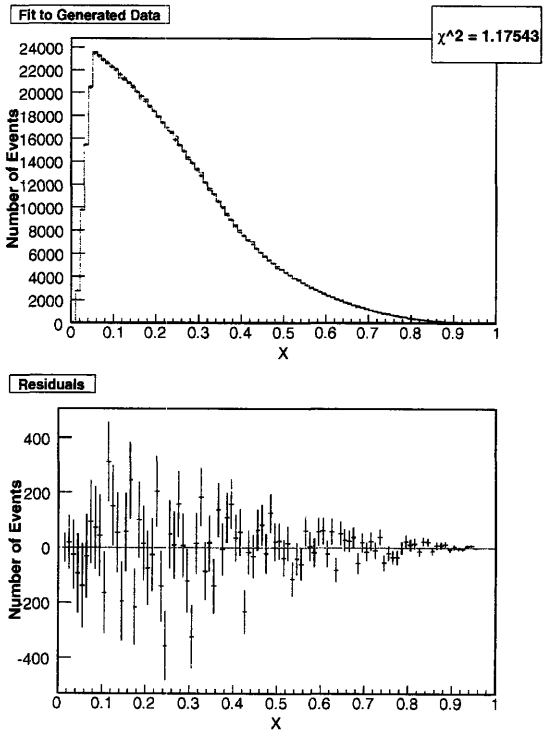


Figure 4-3: Example of the results from a fit.

The two steps to using this approach are calculating the weights of the points being interpolated between during the generation of the fit spectra, and then using these weights to calculate the new weight during the fitting process. During the generation of the fit spectrum, 10 different weights are calculated and stored for each event for values of $\rho$ and $\eta$, as determined from the standard model values and a specified increment size. During the fitting process, the weight for each event for the current values of $\rho$ and $\eta$ is calculated from a polynomial dependent upon the 10 stored weights and the difference in the parameters from their Standard Model values.

## 4.3 Results

The final goal of this study was to examine the relationship between the uncertainty in the detector response function and the uncertainty in the Michel parameters of the fit result. Each detector parameter (ie, resolution, or the maximum efficiency as dependent on energy) was varied independently over a range of values with a number of fits done at each value. For each detector parameter a plot can be made of the error on the Michel parameter fit values as a function of the offset of the detector parameter. For each detector parameter there are 3 plots, corresponding to $\rho$, $\eta$, and the normalization. The data can then be fit to extrapolate the overall relationship between the two parameters.

Each parameter has a specified "nominal" value that was a reasonable estimate for its value in the detector model. Only one of the detector variables were modified at a time, with the remaining variables at their nominal value. The goal is to study the effect of the uncertainty in the detector response, so the parameter is only being modified in the fit spectrum. The data spectrum is always modeled by the nominal values.

For the efficiencies, the nominal maximum efficiency was set to 98%. This allowed the fit to include both higher and lower values, without including the non-physical region above unity. The scale and offset variables were set to 1 and 0, respectively, which would be their optimal values. A priori, there is no reason to choose a value larger or smaller than the optimal, though the true value is likely non-optimal. The values used for the fit were chosen symmetrically around the nominal values, however, the fit response was asymmetric, especially in the case of the offset. 1% was chosen as the nominal resolution value, again allowing variations in both directions within physically allowed values.

All data were fit linearly, except the offset, which was better modeled quadratically (see Appendix A). The parameters of the fit appear on the plots in Appendix A. Error bars represent the variance in the 20 fits done at each value. The y-axis on all of the plots represents the pull value, which is the ratio of the difference between the fit and

| Variable Changed | Parameter | Nominal Value | Pull at Nominal Value | $\Delta$ for $\Delta$y=1 |
|---|---|---|---|---|
| Resolution | $\rho$ | 0.01 | 0.29 $\pm$ 0.37 | 0.013 $\pm$ 0.010 |
| | $\eta$ | 0.01 | 0.33 $\pm$ 0.37 | 0.013 $\pm$ 0.011 |
| | norm | 0.01 | 0.20 $\pm$ 0.69 | 0.043 $\pm$ 0.032 |
| $\theta_{eff}$ | $\rho$ | 0.98 | 0.20 $\pm$0.40 | 5 $\pm$ 130 |
| | $\eta$ | 0.98 | 0.23 $\pm$0.38 | 6 $\pm$ 150 |
| | norm | 0.98 | 0.23 $\pm$0.25 | 0.001211 $\pm$ 0.000010 |
| $E_{eff}$ | $\rho$ | 0.98 | 0.24 $\pm$0.40 | 2 $\pm$ 30 |
| | $\eta$ | 0.98 | 0.20 $\pm$0.41 | 9 $\pm$ 410 |
| | norm | 0.98 | 0.23 $\pm$0.24 | 0.001211 $\pm$0.000002 |
| $\phi_{eff}$ | $\rho$ | 0.98 | 0.23 $\pm$0.28 | 1 $\pm$30 |
| | $\eta$ | 0.98 | 0.24 $\pm$0.39 | 1 $\pm$ 50 |
| | norm | 0.98 | 0.19 $\pm$0.30 | 0.001212 $\pm$ 0.000012 |
| Scale | $\rho$ | 1.0 | 0.28 $\pm$0.41 | 0.00164 $\pm$ 0.00034 |
| | $\eta$ | 1.0 | 0.18 $\pm$0.41 | 0.0042 $\pm$ 0.0023 |
| | norm | 1.0 | 0.098 $\pm$0.29 | 0.082 $\pm$ 0.65 |
| Offset | $\rho$ | 0.0 | 0.19 $\pm$0.38 | 3.11 $\pm$ 0.93 |
| | $\eta$ | 0.0 | 0.15 $\pm$0.39 | 1.81 $\pm$ 0.32 |
| | norm | 0.0 | 0.19 $\pm$0.29 | 4.4 $\pm$ 1.3 |

Table 4.2: Uncertainty in Given Variable for a Change of Fitted Value of 1 Standard Deviation

actual value to the standard deviation of the measurement. Hence, a pull of zero is a perfectly fit parameter and a pull of $\pm 1$ represents $\pm 1\sigma$ from the actual value.

Table 4.2 shows the results of the fit and the corresponding calculations. The pull at nominal value is the y-value of the fitted function, evaluated at the nominal value. This is not necessary what was measured at the nominal value. For a "perfect" fit, this should be zero since all of the parameters would be matched. The final calculation is the change in parameter ($\Delta$) necessary to change the pull by one unit of $\sigma$. This number gives the margin for which we must be able to determine the detector response function parameters to have their systematic error be less than one standard deviation. $\Delta$ is calculated as the change from the nominal value, not from a pull equal to zero. For the linear fits, $\Delta$ is simply dependent upon slope.

## 4.4 Analysis and Conclusions

From the plots of the fits, both quantitative and qualitative statements can be made. The plots clearly show very similar behavior in the three efficiencies and interesting effects in the other three detector variables. The calculations made from the fits allow us to find a relationship between the detector response uncertainty and systematic errors of this type of fit.

The three detector efficiency parameters have very similar behaviors, though each is modeled differently. Over all values studied, there was no statistical difference in the fit of $\rho$ and $\eta$. This is expected due to the efficiencies functioning as a vertical scale factor, but having little influence along the x-axis. All efficiencies have a strong effect on the normalization since a mismatch in efficiency reduces the number of counts in the spectra, which must be compensated by the normalization. In efficiencies that are dependent upon $\phi$ and $\theta$, and change in normalization will be equivalent in the muon and electron spectrum and the ratio will not change. If the energy efficiency is different for muons and electrons, that will have an effect on the ratio.

The effect of the resolution is complicated by the finite bin size of the spectra. When the range of values in one bin is much greater than the resolution, only a negligible number of events would end up in the incorrect bin due to resolution. In the case that the majority of events in a bin lie within 1 or 2 $\sigma_{res}$ of another bin, resolution will have a great effect.

Changing the energy scale results in a relatively linear response in the fit to the Michel parameters. This is reasonable upon examining Eq. 2.4. It has a minimal effect on the normalization. At high energies, where the scaling would have the greatest effect, there are the fewest events.

The detector parameter with the greatest impact on the fit to the Michel parameters $\rho$ and $\eta$ is the energy offset. A mismatch in the energy offset between the model of the detector response function and the actual response by about 2 MeV is enough to have a large effect on the fit of $\rho$, $\eta$, and the normalization. This has a much larger effect than the normalization does since it shifts the events in the lower-energy region

of the spectrum, which is much more dependent upon $\rho$ and $\eta$.

It is essential to minimize the uncertainty in all three detector efficiencies and the energy offset in order to measure the number of events in a spectrum. However, the leptonic branching ratio will not be effected by the uncertainties if the detector efficiencies are equal for muons and electrons. The branching ratio will be effected by the energy offset since the difference in mass between the electron and muon results in a different energy scale (see Eq. 4.1). If the energy offset is equivalent (say, 1 MeV) for electrons and muons, it will result in different shifts when converted to $x = E/E_{max}$. This will result in different changes in normalization which then effect the branching ratio.

# Chapter 5

# Conclusion

From table 4.2 we are able to determine which parameters could adversely affect the fits. The three maximum efficiency values do not affect the fits to $\rho$ and $\eta$, but do strongly affect the normalization values. Any uncertainties in the efficiencies will result in uncertainties in the number of events measured. For the $\theta$ and $\phi$ efficiencies, any scaling due to uncertainties will cancel in the muon and electron spectra. If the energy efficiency is identically modeled for the muon and electron spectra it will similarly cancel. By only using the drift chamber to make measurements, this should be the case. Otherwise, different energy efficiencies will cause different changes in the normalization which then changes the measurement of the branching ratio.

The resolution of the drift chamber system is $\sigma_{p_t}/p_t = (0.45 \pm 0.013)\% + (0.13 \pm 0.01)\%p_t$ [1]. Table 4.2 shows that the uncertainty in resolution needs to be on the order of 1% in order for it to affect the fit. The highest momenta are on the order of 10 GeV/c, so the maximum uncertainty will be about 0.1%. The lower half of the momentum spectrum is the most important to the fit, and the uncertainty will only be on the order of 0.05% there. Hence, uncertainty will not have a large affect on the fit.

The scale value affects both Michel parameters, with a greater sensitivity in $\rho$. An uncertainty in the scale value at the level of 0.1% will result in a shift in the fit to $\rho$ by 1 $\sigma$. Measurements show an energy scale uncertainty on the order of 0.05%, low enough to not have a sizable effect on the fit [1]. The energy offset also has a large

impact in the Michel parameters. An uncertainty in the energy measurement over about 1.5 MeV could cause the fit of the Michel parameters to be off by one standard deviation.

The energy offset will affect the ratio of the leptonic branching fractions due to the different energy scales of the two leptons. Even if the offset is equal for both muons and electrons it will cause different shifts in the normalization, leading to a change in the ratio of the branching fractions. While other parameters affect normalization, this is the only one that cannot possibly cancel when the ratio of the events is taken.

In conclusion, uncertainties in the efficiencies will result in uncertainties in the number of events measured. The uncertainty in energy efficiency will not affect the branching ratio if it is modeled the same way for electrons and muons. The energy offset and scale affect the fit to the Michel parameters. The energy offset will not cancel between the muon and electron spectrum in calculating the branching ratio, so it the most important parameter to control to calculate the branching ratio.

# Appendix A

# Pull Plots

These plots show the effect of a mismatch between the parameters for the data and fitting spectra. For each plot only one variable was considered.

| Parameter | Notation | Value |
|---|---|---|
| Number of events in fitting spectrum | N | 1,000,000 |
| Number of events in data spectrum | M | 50,000,000 |
| Standard Model value for $\rho$ | $\rho_s$ | 0.75 |
| Standard Model value for $\eta$ | $\eta_s$ | 0.0 |
| Normalization | nrm | M/N |
| Number of bins | | 100 |
| $\rho$ increment for weight generation and fitting | $\delta\rho$ | 0.05 |
| $\eta$ increment for weight generation and fitting | $\delta\eta$ | 0.05 |
| Normalization increment for fitting | $\delta$nrm | 0.01 |
| Energy Efficiency | $E_{eff}$ | 0.98 |
| $\theta$ Efficiency | $\theta_{eff}$ | 0.98 |
| $\phi$ Efficiency | $\phi_{eff}$ | 0.98 |
| Resolution | res | 0.01 |
| Energy Offset | off | 0 MeV |
| Energy Scale Factor | scale | 1 |

Table A.1: Parameters used to study effects of detector uncertainties.

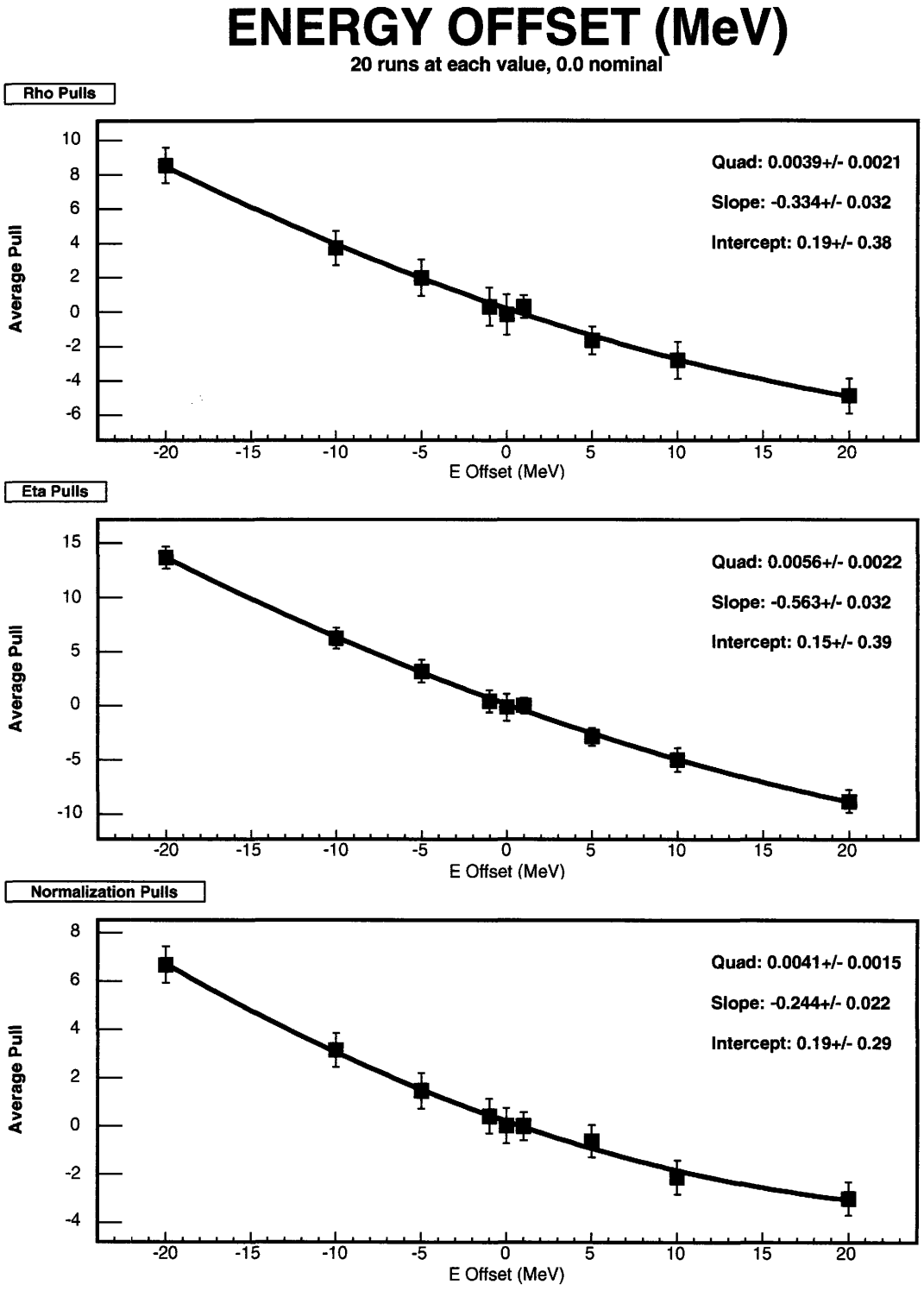


Figure A-1: How the fit changes as the energy offset is changed.

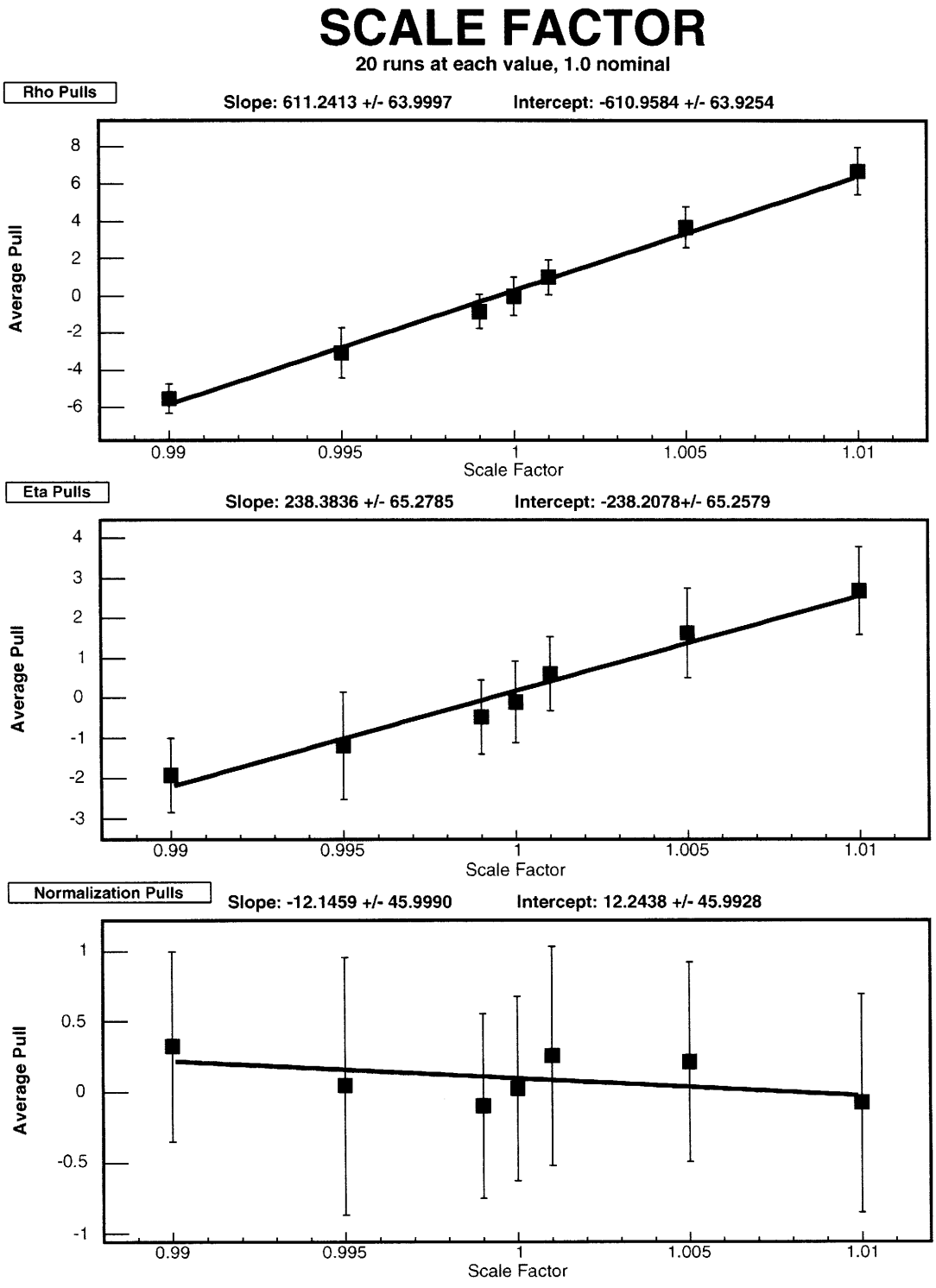


Figure A-2: How the fit changes as the scale factor is changed.

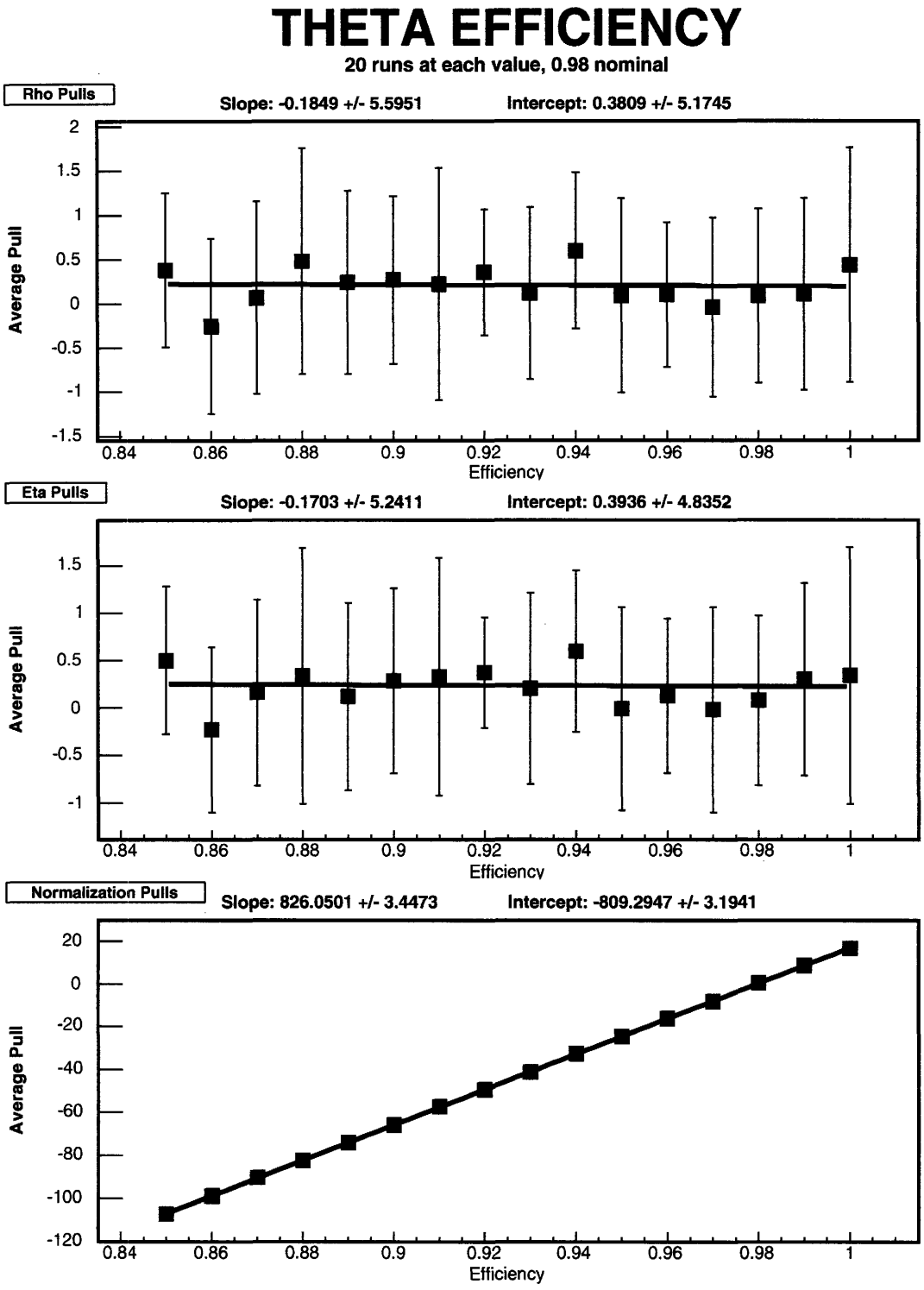


Figure A-3: How the fit changes as the efficiency as a function of theta is changed.

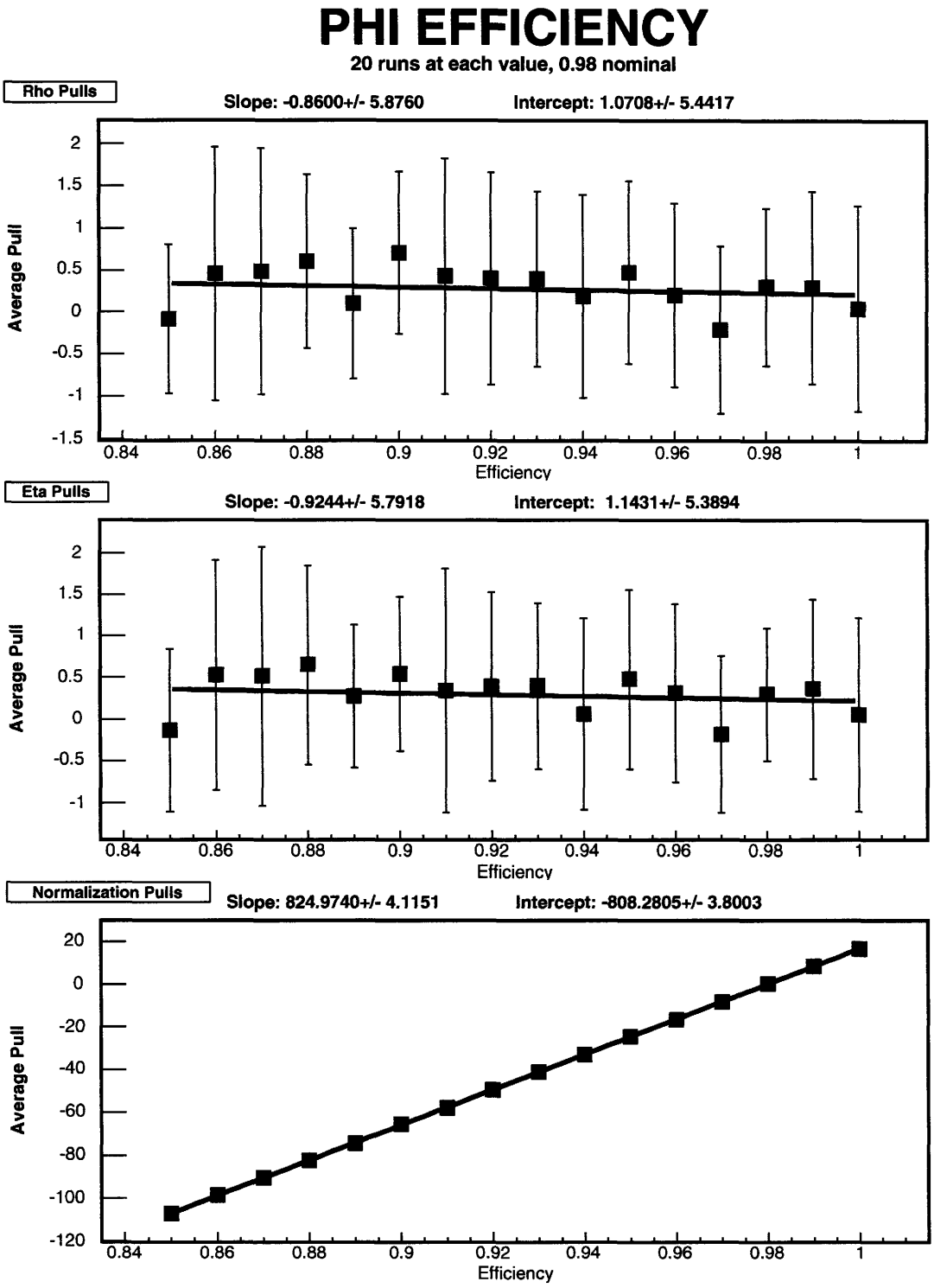


Figure A-4: How the fit changes as the efficiency as a function of phi is changed.

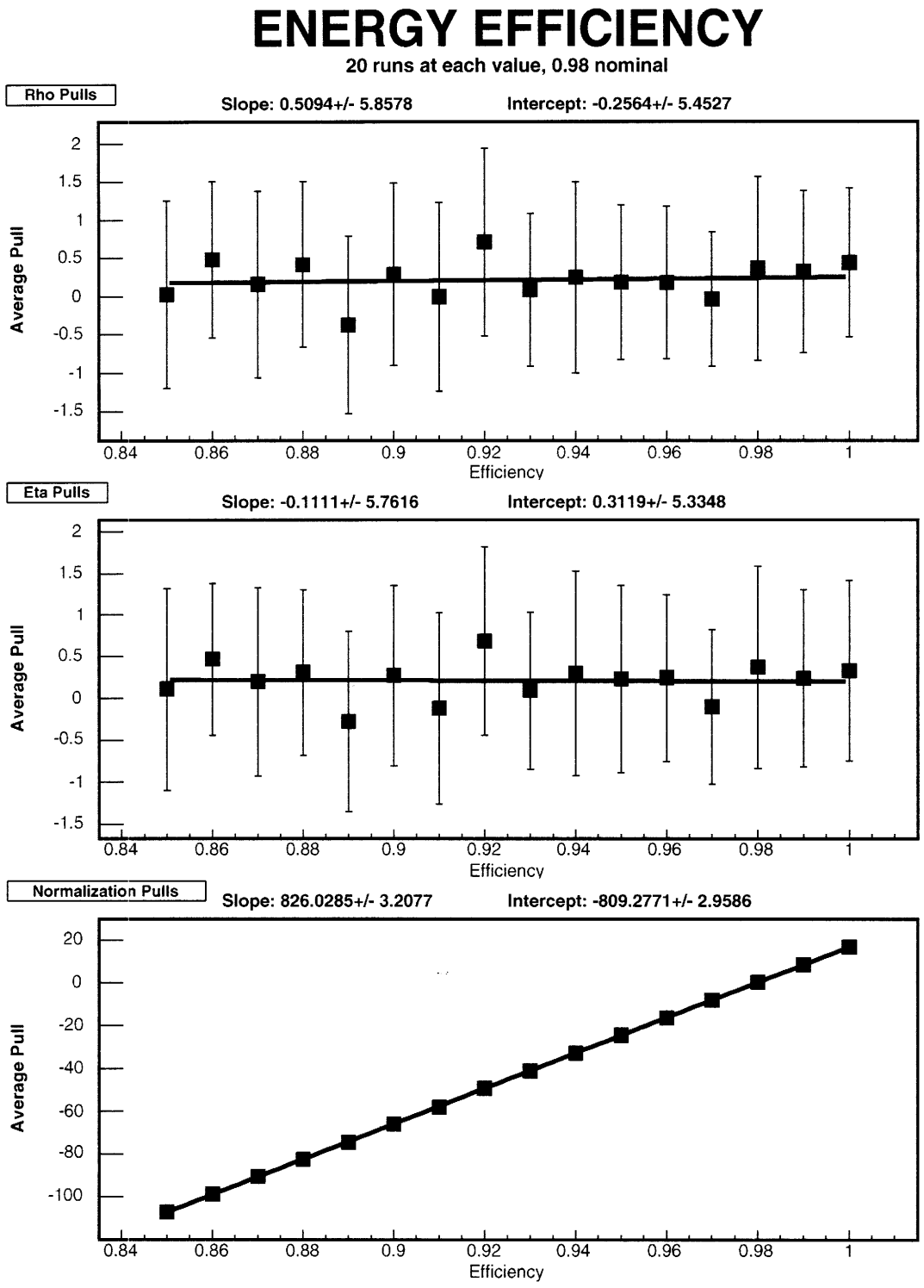


Figure A-5: How the fit changes as the efficiency as a function of energy is changed.

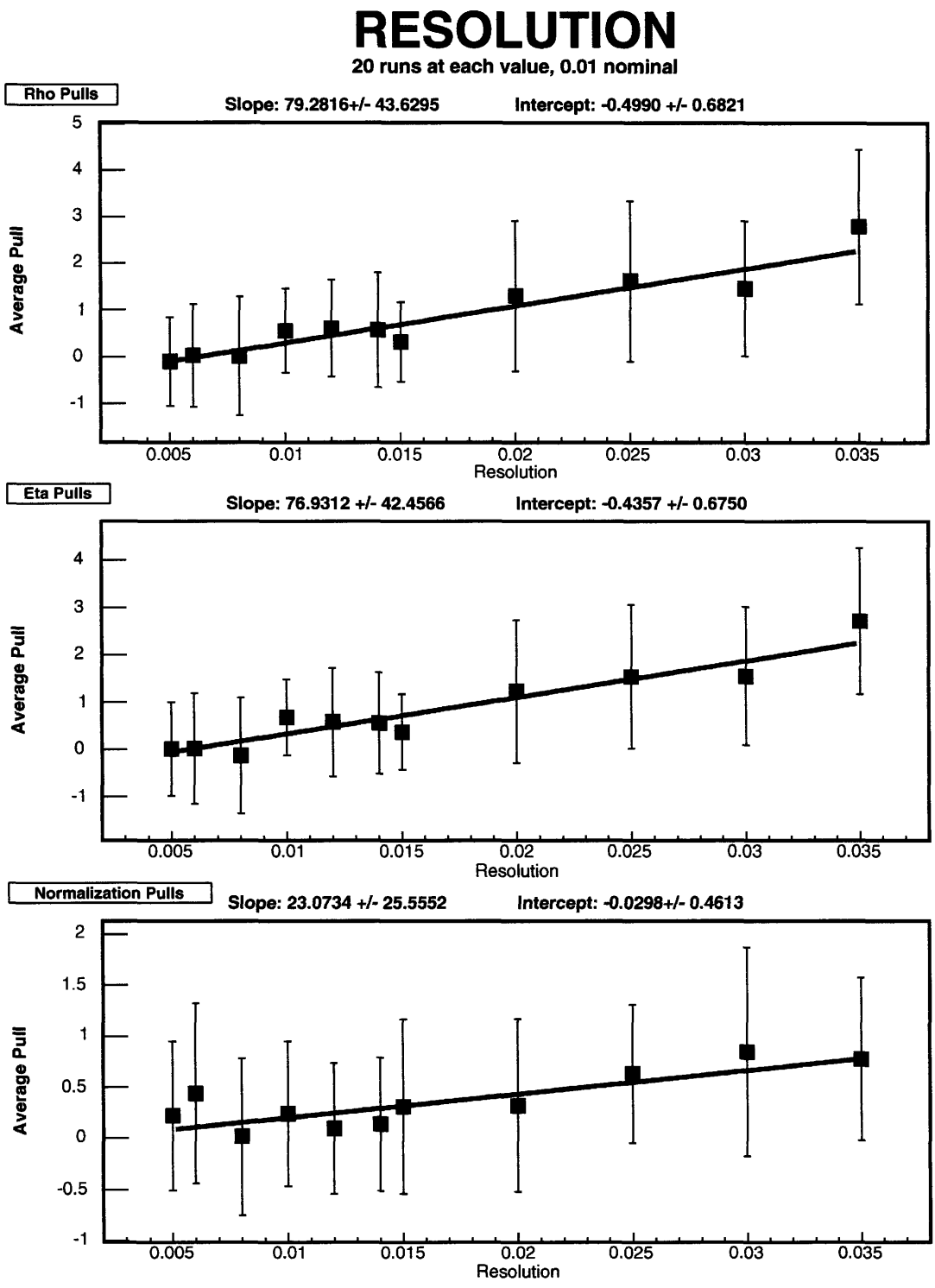


Figure A-6: How the fit changes as the resolution value is changed.

# Bibliography


[1] **BABAR** Collaboration, B. Aubert *et al.*, "The BaBar detector," *Nucl. Instrum. Meth.* **A479** (2002) 1–116, hep-ex/0105044.

[2] W.-M. Yao *et al.*, "Review of Particle Physics," *Journal of Physics G* **33** (2006) 1+.

[3] D. I. Kazakov, "Beyond the standard model," hep-ph/0611279.

[4] W. Loinaz, N. Okamura, T. Takeuchi, and L. C. R. Wijewardhana, "The NuTeV anomaly, neutrino mixing, and a heavy Higgs," *Phys. Rev.* **D67** (2003) 073012, hep-ph/0210193.

[5] W. Loinaz, N. Okamura, S. Rayyan, T. Takeuchi, and L. C. R. Wijewardhana, "The NuTeV anomaly, lepton universality, and non-universal neutrino-gauge couplings," *Phys. Rev.* **D70** (2004) 113004, hep-ph/0403306.

[6] A. Stahl, "The Michel parameter eta in tau decays," *Phys. Lett.* **B324** (1994) 121–124.

[7] **OPAL** Collaboration, K. Ackerstaff *et al.*, "Measurement of the Michel parameters in leptonic tau decays," *Eur. Phys. J.* **C8** (1999) 3–21, hep-ex/9808016.

[8] **CLEO** Collaboration, R. Ammar *et al.*, "A measurement of the Michel parameters in leptonic decays of the tau," *Phys. Rev. Lett.* **78** (1997) 4686–4690.

[9] G. D. Lafferty, "Tau Physics from B Factories," hep-ex/0610028.

[10] C. Brown and M. Roney, "A Study of the Leptonic Branching Ratios of the Tau at BaBar." BaBar Analysis Document 309, Version 1.

[11] M. L. Perl *et al.*, "Properties of Anomalous e mu Events Produced in e+ e- Annihilation," *Phys. Lett.* **B63** (1976) 466.

[12] Y.-S. Tsai, "Decay Correlations of Heavy Leptons in e+ e- $\rightarrow$ lepton+ lepton-," *Phys. Rev.* **D4** (1971) 2821.

[13] B. Povh, K. Rith, C. Scholz, and F. Zetsche, *Particles and Nuclei: An Introduction to the Physical Concepts.* Springer, 2004.

[14] F. Halzen and A. D. Martin, *Quarks and Leptons: An Introductory Course in Modern Particle Physics.* John Wiley and Sons, 1984.

[15] **NuTeV** Collaboration, G. P. Zeller, "A departure from prediction: Electroweak physics at NuTeV," hep-ex/0207037.

[16] L. Michel, "Interaction between four half spin particles and the decay of the mu meson," *Proc. Phys. Soc.* **A63** (1950) 514–531.

[17] A. Rouge, "Tau lepton Michel parameters and new physics," *Eur. Phys. J.* **C18** (2001) 491–496, hep-ph/0010005.

[18] J. Seeman *et al.*, "A luminosity of $10^{34} cm^{-2} s^{-1}$ in the PEP-II B- factory.". Contributed to European Particle Accelerator Conference (EPAC 06), Edinburgh, Scotland, 26-30 Jun 2006.

[19] **BABAR Drift Chamber** Collaboration, G. Sciolla *et al.*, "The BaBar drift chamber," *Nucl. Instrum. Meth.* **A419** (1998) 310–314.

[20] J. Albert *et al.*, "Electronics for the BaBar central drift chamber," *IEEE Trans. Nucl. Sci.* **46** (1999) 2027–2032.

[21] **BABAR** Collaboration, M. H. Kelsey, "Performance and aging of the BaBar drift chamber," *Nucl. Instrum. Meth.* **A535** (2004) 206–211.

[22] P. Garcia-Abia, "Measurement of the tau lifetime and leptonic branching ratios in L3," *Nucl. Phys. Proc. Suppl.* **98** (2001) 75–84.

[23] G. Lynch, S. Schaffner, S. Wagner, G. Raven, and F. Wilson, "BaBar Drift Chamber Tracking Conventions." BaBar-Note 488, April, 1999.

[24] F. James and M. Roos, "'MINUIT' A System for Function Minimization and Analysis of the Parameter Errors and Correlations," *Comput. Phys. Commun.* **10** (1975) 343–367.

[25] R. Brun and F. Rademakers, "ROOT: An object oriented data analysis framework," *Nucl. Instrum. Meth.* **A389** (1997) 81–86.